


Electrokinetic Control of Viscous Fingering in a Perfect Dielectric Fluid

Benedicta N. Nwani[✉], Anjali Patadia,[†] Ian D. Gates[✉], and Anne M. Benneker^{✉*}

Department of Chemical and Petroleum Engineering University of Calgary 2500 University Drive Northwest, Calgary, Alberta T2N 1N4, Canada

 (Received 2 November 2021; revised 13 May 2022; accepted 27 July 2022; published 12 September 2022)

Viscous fingering (VF) is a well-known interfacial instability occurring when a viscous fluid in a porous medium is displaced by a lower viscosity fluid. In this work, we show that electrokinetic control of the instability is possible, even in the case of a perfect dielectric viscous defending fluid. Using Hele-Shaw cell experiments in which a nonconducting viscous mineral oil is displaced by a conducting less viscous brine solution, we observe that we are able to effectively control the stability of the interface. We evaluate the interfacial stability at different field strengths, both positive and negative with respect to the pressure-driven flow and find that an electric field in the same direction as the pressure-driven flow significantly stabilizes the interface. In contrast, an electric field opposing the pressure-driven flow further destabilizes the displacement. We attribute this to the interplay between the different ζ potentials (fluid-fluid and fluid-wall) and preferential oil wettability of the system, resulting in the formation of an oil-film layer throughout the displacement. The nonconducting mineral oil in our system acts then as a dead-end pore for the brine, which under the influence of an electric field develops an electro-osmotic flow velocity. We qualitatively and quantitatively show that for all positive electric field strengths VF is reduced, while for negative electric fields VF is increased and that the electric field strength has limited influence on the degree of (de)stabilization. The results from this work are of particular relevance in applications where VF occurs in a system containing one nonconducting fluid, which are common in many applications such as enhanced oil recovery.

DOI: [10.1103/PhysRevApplied.18.034029](https://doi.org/10.1103/PhysRevApplied.18.034029)

I. INTRODUCTION AND BACKGROUND

Viscous fingering (VF), an interfacial instability, which occurs when a high viscosity fluid (μ_1) is displaced by a lower viscosity fluid (μ_2) in a porous medium, is a phenomenon that is relevant for applications such as water flooding [1–5], CO₂ storage in saline pore fluids [6–10], spreading of pollution zones in aquifers [11,12] as well as the expansion of bands in liquid chromatography for the separation of chemical species in a sample [13–15]. In many applications, VF is undesirable and thus needs to be controlled. Passive control methods, in which no *in operando* dynamics are employed, can involve the use of elastic substrates [16–18], wettability modification [19–22], geometrical heterogeneity [23–25] and the use of tapered control volume geometries [26–30]. All passive control methods for VF are implemented prior to the start of the process. On the other hand, active control methods are employed *in operando* and are controlled externally by dynamically changing process parameters.

Examples of active control include the adjustment of the flow rate or geometry [31–34] and the use of an electric field [35,36]. Electrokinetic control of VF, in which an external electric field is applied over the porous domain, is a relatively unexplored method, but shows promising results for systems with two electrolytes [35,36]. Charges in the system result in the development of an electric double layer (EDL), on which the external electric field acts, inducing electro-osmotic flows (EOF) in systems containing two perfectly conducting fluids. For two immiscible electrolytes of equal conductivity where the fluid with higher EOF velocity (as a result of the fluids permittivity, ζ potential, and viscosity) is displaced by an electrolyte with lower EOF velocity, EOF in the same direction as the pressure-driven flow has been shown to effectively stabilize VF. In the case of a viscous perfect dielectric resident fluid, the emergence of an EDL in that fluid is suppressed, and the effect of an electric field is increasingly complicated as a result of the emergence of a net charged liquid-liquid interface. In this work, we experimentally investigate the electrokinetic control of VF in systems where the defending fluid is a more viscous nonconducting mineral oil, which is a case relevant for many applications such as enhanced oil recovery (EOR) and find that even if the resident fluid is nonconducting, the

*anne.benneker@ucalgary.ca

[†]Department of Mechanical Engineering University of Calgary 2500 University Drive Northwest, Calgary T2N 1N4, Alberta, Canada.

application of an electric field can effectively suppress VF. We show that, even for relatively low field strengths, this interfacial phenomenon can be effectively controlled.

A. Theoretical background

In the case of a conducting and nonconducting fluid (e.g., water and oil) in contact with the same solid, two different effective ζ potentials are obtained [37]; (1) between the conducting fluid and the wall, ζ_{fw} and (2) between the conducting and nonconducting fluid, ζ_{ff} . The ratio of these ζ potentials $Z_r = |\zeta_{ff}/\zeta_{fw}|$ is of influence on the fluid flow under an electric field. When $Z_r = 0$, which is the case for two electrolytes of the same conductivity, the fluid-fluid interface can be considered electrically neutral and would not experience a force under the influence of an externally applied electric field, such that it has negligible influence on the interface motion. Any nonzero value for Z_r implies that there is a charge on the interface, and thus an applied electric field will act on the fluid-fluid interface as well as on the fluid-solid interface, influencing the overall EOF in the system. In the case of $Z_r > 1$, the fluid-fluid interface has a significantly large charge, is of the same sign as the fluid-wall interface, and the motion of this fluid-fluid interface will dominate over the EOF induced on the fluid-wall interface. On the other hand, when $Z_r < 1$, the hydrodynamics are expected to be dominated by the fluid-wall EOF, but the effects of the fluid-fluid interface are non-negligible [37]. Previous studies have shown that electrically charged fluid-fluid interfaces can modify the applied electric field, the interfacial tension (IFT) between the fluids and also change the interfacial pattern [38]. Numerical works of Bensimon [39] have shown that for the cases where IFT values are low, the interface exhibits nonlinearities such as tip splitting, while a high IFT value would have a stabilizing effect on the interface. Other effects, such as the wettability of the system for both fluids also influence the development of interfacial instabilities [36,40–43]. If the system is preferably wet by defending fluid, a film may occur at the solid wall, and the invading fluid will not be in ideal contact with the wall [19]. These effects have an influence on the development of the EDL and thus on the EOF expected in the system.

A combination of pressure-driven flow and electrokinetic flow results in an overall fluid movement and ionic flux. The ionic current is due to the streaming and Ohmic currents from the pressure gradient and potential gradient, respectively. When the fluids in the system are electrolytes of the same conductivity, both the fluid and ionic fluxes are continuous across the fluid-fluid interface. Therefore, in the case of an electrically neutral interface ($Z_r = 0$), the forces on the fluid-fluid interface can be neglected and the transport and interfacial stability are depending on EOF along the channel walls. The direction of the applied external electric field influences the stability of the interface. In

the case of a negatively charged wall, and thus an excess of positive charges in the EDL, an electric field in the direction opposite to the pressure-driven flow (referred to as a negative electric field) is expected to drive EOF towards the fluid inlet. On the other hand, an electric field applied in the same direction as the pressure-driven flow (a positive electric field) EOF in the conducting phase is expected to be towards the outlet. The net velocity profile between the two walls is a combination of EOF and pressure-driven flow, and depending on the applied field strength and the wall charge, the overall velocity profile changes and the overall displacement is altered.

For the case of two electrolytes with electrically neutral interface, $Z_r = 0$, the electric field strength required for stabilization depends on the fluid viscosities, permittivities, conductivities, wall potential in the fluids and the fluid injection velocity U . A critical electric field value can be obtained for full interfacial stabilization; $E_{\text{crit}} = [((\mu_1 - \mu_2)U)/(\epsilon_2\zeta_2 - \epsilon_1\zeta_1)]$ [35]. This direction of the electric field is depending on the combination of the magnitude of $\epsilon_1\zeta_1$ and $\epsilon_2\zeta_2$, where if $|\epsilon_2\zeta_2| < |\epsilon_1\zeta_1|$, the field should be positive with a magnitude larger than E_{crit} , while if $|\epsilon_2\zeta_2| > |\epsilon_1\zeta_1|$, the field should be negative with a magnitude smaller than E_{crit} .

In this work, we consider a rectilinear Hele-Shaw cell with a cell gap h and negatively charged walls, which is initially filled with a wetting nonconducting mineral oil with viscosity μ_1 , conductivity σ_1 , and permittivity ϵ_1 (Fig. 1). This is a significantly different system than the case of two electrolytes described above. When displacing this fluid using a purely pressure-driven electrolyte flow ($\mu_2 < \mu_1$, $\sigma_2 \gg \sigma_1$ and $\epsilon_2 > \epsilon_1$), interfacial instabilities are expected because of the unfavorable viscosity ratio ($\mu_2/\mu_1 < 1$) [Fig. 1(a)]. Because of the zero electrical conductivity and the absence of ions, ζ_1 , the wall potential exhibited in the nonconducting fluid will be negligible, and although any applied electric field can pass through the fluid, no significant EOF is expected in this fluid [Fig. 1(b)]. The effective ζ potential between the electrolyte and solid wall, ζ_2 , is significantly larger than ζ_1 , and an external electric field will induce a body force on the EDL between the walls and electrolyte. In this case, it is expected that there are significant deviations from the case of two electrolytes. Various authors [44,45] have shown that the sudden change in ζ potential (i.e., surface-charge discontinuity) typically found during the displacement of nonpolar oil with brine can induce flow and internal pressure gradients within the system. This internally built-up pressure gradient can cause acceleration or deceleration of flow in the presence of an externally applied electric field. These induced pressure gradients make the velocity profile deviate from the plug-flow profile [45] such that a “stable” interface may still have a single finger formed in which the width of the single finger occupies at least half of the displacement domain [1]. Further, it has been

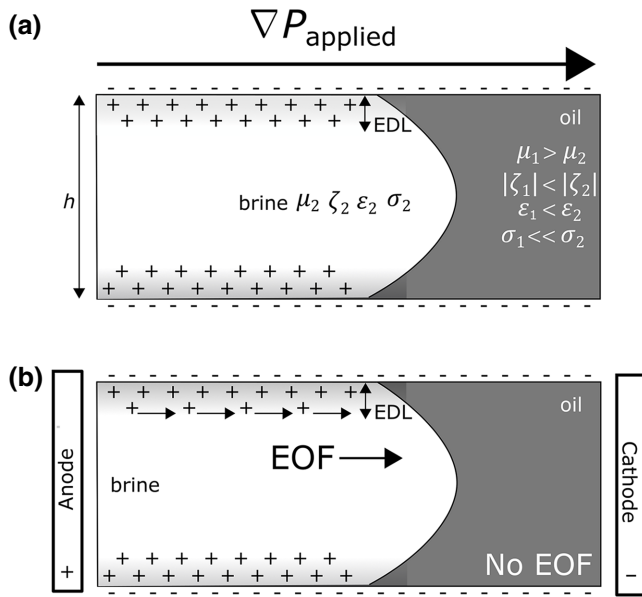


FIG. 1. Schematic side-view representation of the EDL and developed EOF in the Hele-Shaw cell (with thickness h) where a nonconducting resident fluid is present. The pressure-driven flow is from left to right. (a) Base case, without an electric field. The brine and oil have significantly different electrical properties. The negative wall charge gives rise to a positively charged EDL, solely in the brine phase. Hydrodynamically unstable as a result of the unfavorable viscosity ratio. (b) Upon application of an electric field (anode at the inlet, cathode at the outlet), the charges in the brine EDL will move towards the electrode of opposite sign, inducing an electro-osmotic flow. Since the oil is nonconducting and no EDL is present, no EOF develops in the oil phase and the relative velocities between the two phases changes, leading to a pressure buildup in the brine phase. Note, the shape and size of the interface and EDL are not to scale, in this drawing we neglect the change of interface as a result of the electric field. These effects are elaborated upon in Fig. 4.

noted that during a combination of pressure-driven and EOF, the pressure gradient must adjust to compensate for the EOF [35,36], while other studies [46] have found that when there is a competition between EOF and pressure-driven flow, an electric field applied in the same direction to flow results in an adverse effect on the pressure gradient such that it causes a backward pressure flow resulting in a flow reversal. For the case of a viscous perfect dielectric invaded by a conducting brine, EOF induced in the same direction as flow could therefore induce a local pressure buildup in the system [45], as if the invading fluid was encountering a dead end shown in Fig. 1(b), as well as in Fig. 4(b). This dead-end effect makes the fluid act as though the IFT between them is increased, thereby making the fluid propagation more stable. Further, the total flux is reduced at the interface given that the flux due to current is blocked by the oil phase, which in turn further controls the interface motion. Therefore, in the case of a nonconducting more viscous resident fluid, a positive

electric field is expected to stabilize the system, while a negative field is expected to induce further instabilities. This increased instability as a result of the negatively applied electric field is attributed to a combination of factors, including (1) the preferential resident fluid wetness of the cell, (2) the apparent thickening of the resident fluid under the influence of the negatively applied electric field, which then makes the viscosity ratio even more unfavorable, and finally, (3) the increased pressure gradient due to the thickening of the resident fluid, which in turn facilitates the invasion of the displacing fluid. The increased invasion of the displacing fluid then makes the fluid-fluid interface act as though there is a reduction in the effective interfacial tension and results in a further destabilization of the interface.

II. EXPERIMENTAL METHODS

A schematic of our experimental setup is shown in Fig. 2. Our experimental setup consists of a rectilinear Hele-Shaw cell made from acrylic (polymethyl methacrylate, PMMA), with a length of 15 cm and a width of 11.5 cm. The field of view has a length of 8 cm and width of 6.9 cm. The PMMA sheets have a thickness of 1.5 cm to prevent any bending in the system. The characteristic thickness of the channel h is dictated by a plastic shim stock with a thickness of 101.6 μm . Ports for fluid injection, pressure monitoring, and electric field application are located in the inlet and outlet of the cell. Two syringe pumps were used to pump the fluids into the system at the desired flow rate of 0.05 ml/min, corresponding to a capillary number $Ca = \mu_1 U / \gamma_{1,2} = 1.13 \times 10^{-4}$, where $\gamma_{1,2}$ is the interfacial tension between both fluids, measured to be 46 mN/m. An electric potential is applied through brass sheets, embedded in the top of the cell, spanning the total width of the cell to ensure an evenly distributed field. A 5-kV Keithley 2290-5 dc power supply is used to apply the electric field. A LED light box is placed beneath the cell for illumination and a Basler scA 1000-30fc CCD camera with 30fps is mounted perpendicularly above the set up for capturing the images during the experiments. All equipment is controlled using LabVIEW and data is recorded simultaneously to image acquisition. Before each experiment, air is evacuated with a vacuum pump to ensure that there are no air bubbles introduced during the fluid displacement.

In the experiments, a 1.4-mM NaCl solution with a viscosity of 1.07 mPa s, conductivity of 246.7 $\mu\text{S}/\text{cm}$, and pH of 5.56 is used to displace a more viscous (55.98 mPa s) and nonconducting light mineral oil of 0 $\mu\text{S}/\text{cm}$ conductivity, obtained from Fisher Scientific. The brine is colored using an electroneutral plant-based blue food colorant from Ward's science to allow for observation of the different phases, which are both colorless by nature. Three situations of the electric field are investigated: (1) base case in which

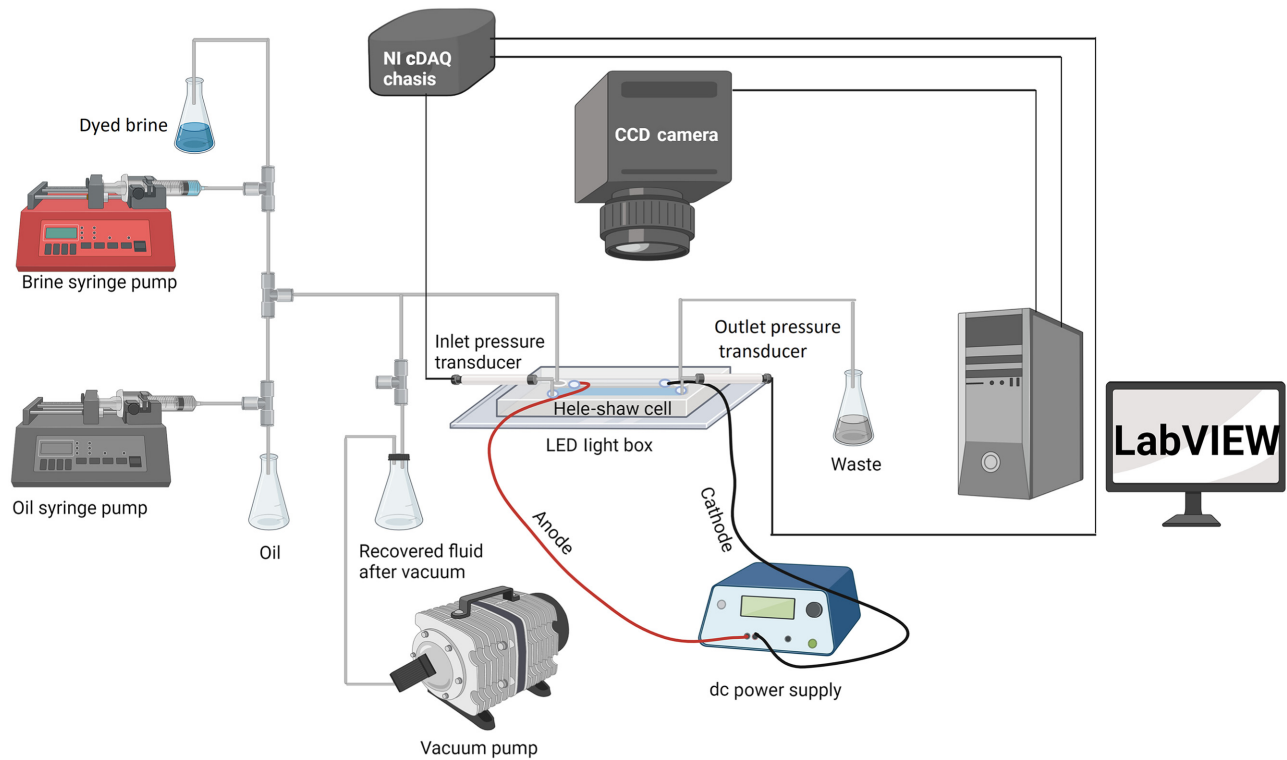


FIG. 2. Experimental setup, consisting of a Hele-Shaw cell connected to two micropumps and a dc power supply. LED illumination ensures the quality of the images captured by the CCD camera. The entire system is controlled using LabVIEW.

the flow is purely pressure driven, (2) pressure-driven flow with a negative electric field, and (3) pressure-driven flow with a positive electric field. In our system, a positive electric field implies the anode is situated at the inlet region, whereby the electric field is in the same direction of flow from the anode to the cathode, while a negative electric field implies that the anode is at the outlet region whereby the electric field in the direction opposite to the pressure driven flow.

For all experiments with electric field, the electric field is applied 30 s after displacement began for two reasons: (1) having brine propagate into the cell before the application of the electric field would ensure that there is a conducting fluid present within the cell (2) to allow for the finger propagation into the system before getting influenced by the applied electric field. All experiments are repeated at least three times to confirm their reproducibility and allow for statistical analysis of the displacement phenomena. Patterns are similar for the repeated runs and therefore, only the results obtained from one of the runs in each experiment are presented here.

To fully understand the results obtained from the displacement experiments, we characterize our system in terms of wall potentials, contact angles, and the direction of EOF in the system. We also investigate the fluid-fluid ζ potential to unravel Z_r for our system. The wettability of the PMMA is characterized using a Krüss Advance

30 DSA. Results showed an increased affinity for oil over water; the oil-solid contact angle is 37.3° while the contact angle of the 1.4 mM NaCl brine-solid is 83.6° . This implies that the cell is preferably oil wet, and that thus the displacement is complicated by a potential interfacial oil layer between the brine and the walls.

The fluid-fluid ζ potential is measured using the method stipulated by Mahani *et al.* [47], where a ratio 1:5 oil-dyed brine volume is sonicated for 20 min in a sonicator bath and allowed to equilibrate for 24 h before ζ -potential measurement is done using the Malvern Zeta Sizer nano. The ζ potential at the oil-brine interface is $\zeta_{ff} = -0.72 \text{ mV} \pm 0.29$, indicating a relatively low interfacial charge. For the wall, the ζ potential is estimated based on previous experiments. Falahati *et al.* [48] showed that the room-temperature ζ potential of PMMA in NaCl brine with an ionic strength between 0.005 and 0.1 M at pH = 4 is approximately -55 and -27 mV, respectively. The experimental work of Walker *et al.* [49] at ambient temperature showed that the ζ potential of acrylic in 0.01 M of KCl brine is around -10 mV at pH = 5.5. Khademi *et al.* [50] has shown that the ζ -potential values of PMMA at pH = 9 are around -70 , -45 , and -40 mV, respectively, for NaCl brine with concentration values of 3, 30, and 100 mM. From these experiments, we conclude that with increasing acidity and increasing brine concentration the absolute value of the ζ potential decreases and the

interface becomes less charged. Based on our system's characteristics, we anticipate the ζ potential of our PMMA in 1.4-mM NaCl brine to be between -5 and -70 mV, depending on the local acidity. Furthermore, based on the small ratio $Z_r = \zeta_{ff} / \zeta_{fw}$ in our system, we conclude that EOF in our system should be dominated by the wall-fluid EOF even though the fluid-fluid interface has a net nonzero charge and therefore will experience forces induced by the externally applied electric field [37].

Based on the ζ -potential estimations, we estimate the theoretically required critical-field strength [35] for interface stabilization using our system parameters. To do this, we first perform a sensitivity analysis to determine how the required critical field for interface stabilization or destabilization would change depending on the ζ -potential values of PMMA reported in the literature [48–51]. In our system, since our oil phase contains absolutely no salt, we assume a zero ζ potential of the PMMA in mineral oil. Measurements of the fluid-fluid ζ potential confirmed that low to zero wall potentials are to be expected for the nonconducting oil phase. Results of this sensitivity analysis show (see Table I in Appendix B) that required field strengths for stabilization are in the order of 10^4 and 10^3 V/cm for ζ -potential values between -5 and -70 mV, respectively, and for a flow rate of 0.05 ml/min. These high values are

a direct result of the restricted contributions of the EOF in the oil phase, where there is an effectively zero wall charge. Experimentally and in applications, these field strengths are infeasible, and thus we investigate the possibility of interface stabilization at a variety of electric field strengths at a flow rate of 0.05 ml/min. We investigate the interface stability for both positive and negative electric field strengths of 150, 300, and 600 V/cm and compare these situations to purely pressure-driven flow.

III. RESULTS AND DISCUSSION

Figure 3 shows the development of patterns and fingering as a function of time in our experiments, for different values of the applied electric field. The invading fluid (white in the figures) is the electrically conducting brine, while the defending fluid (black in the images) is the nonconducting mineral oil. In the case of a purely pressure-driven flow, the development of fingers is observed [Fig. 3(d)]. Under the influence of an external electric field, we see clear alterations of the interfacial behavior, which are significantly different from what is expected in the case of two immiscible electrolytes of the same conductivity, where positive electric fields are expected to further destabilize a hydrodynamically

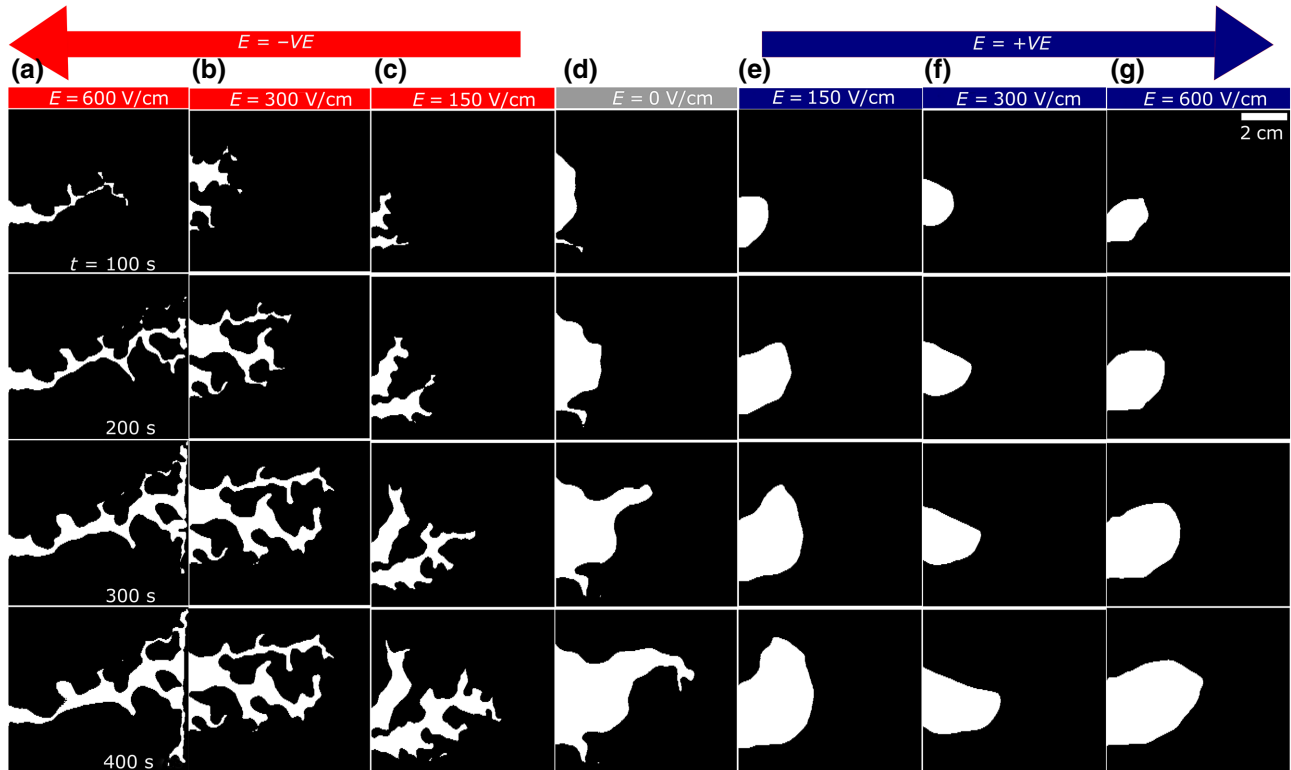


FIG. 3. Qualitative results for all electric field values. Figures (a)–(c) are the patterns gotten for $E = -600$, -300 , and -150 V/cm, respectively, at different time steps. Figure (d) is for purely pressure-driven flow and (e)–(f) are the patterns obtained for $E = +150$, $+300$, and $+600$ V/cm, respectively, at different time steps. Application of a negative electric field [(a), (b) and (c)] shows a qualitative increase of VF when compared to the base case (d), while application of a positive electric field [(e), (f), and (g)] reduces VF.

unstable system, given that the resident fluid has a lower EOF. In our experiments, for all negative electric fields (EOF induced towards the inlet), the interface is destabilized as shown in Figs. 3(a)–3(c) while for all positive electric fields the interface is significantly stabilized in our system as shown in Figs. 3(e)–3(g). In none of the experiments did we observe a full pistonlike displacement, which we attribute to negligible EOF in the oil phase as well as the wettability properties of the cell, which is preferentially oil wet. The effect of the electric field is, however, significant at all electric field values investigated, as can be qualitatively observed in the displacement patterns shown in Fig. 3.

Our results indicate that in the situation where the highly viscous defending fluid is nonconducting, an electric field can still yield suppression of VF. In the case of a negative wall charge, the VF is suppressed under the application of a positive electric field, which induces EOF towards the outlet.

To explain these observations, we calculate the overall interfacial velocity of the brine moving into the oil phase. Our system has a negative wall charge, indicating positive charges in the EDL and implying the direction of EOF to be towards the cathode. As the total velocity in our system comprises of the pressure-driven velocity u_p and the resultant EOF velocity u_{EOF} , we expect the velocity of the interface to increase in the case of a positive field and decrease under a negative field. Our experimental observations, however, indicate the exact opposite behavior, where we observe that for a negative electric field, or having the cathode at the inlet, the interfacial velocity is not negatively impacted and is even slightly increased when compared to a purely pressure-driven flow. On the other hand, when we have a positive electric field, with the anode at the inlet the overall interfacial velocity significantly decreases. We explain this by the complexity of the charges in our system, where in the oil phase there are no charges present and thus the effective charge of the oil-wall EDL is zero, meaning there is a large drop in effective wall charge over the oil-water interface, which then influences the total flux in the system. Recent research has shown that in this case, where the effective wall charge is changing significantly, considerable alterations in fluid-flow behavior from expected EOF can be observed [44,45]. Under the influence of a pressure gradient and an electric field, the conducting interface is fully excluded and flow is directed around the charged interface. Thus, as a result of the significant change in local wall potential, the flow in our system is altered. For the case of a positive electric field, we postulate that the resident oil, which has a zero EO mobility, acts as a significant resistance towards the induced EOF in the brine phase in the direction of the electric field. The resident oil then acts as a “wall” and a pressure gradient is built up in the brine phase, as if it were in a dead-end pore. As a result of this, the brine experiences

a back pressure, which effectively increases the interfacial tension between both fluids, reduces the interfacial velocity and hence, reduces the total mass flux in the system, which we observe as the deceleration of the invading brine phase, that finally reduces the VF. In the case of a negative electric field, EOF in the brine phase is towards the cathode at the inlet of the cell, and the increased instability is attributed to the increased resistance to flow (thickening) of the resident fluid under the influence of the applied electric field. This enhanced resistance to flow of the resident fluid increases the overall pressure gradient in the system, such that the motion of the invading fluid is accelerated, which then causes displacement to act as though the effective interfacial tension is reduced, and hence triggers further instability.

The mechanisms under the different applications of an electric field are schematically depicted in Fig. 4. All figures show a side view of the cell, with the gap thickness

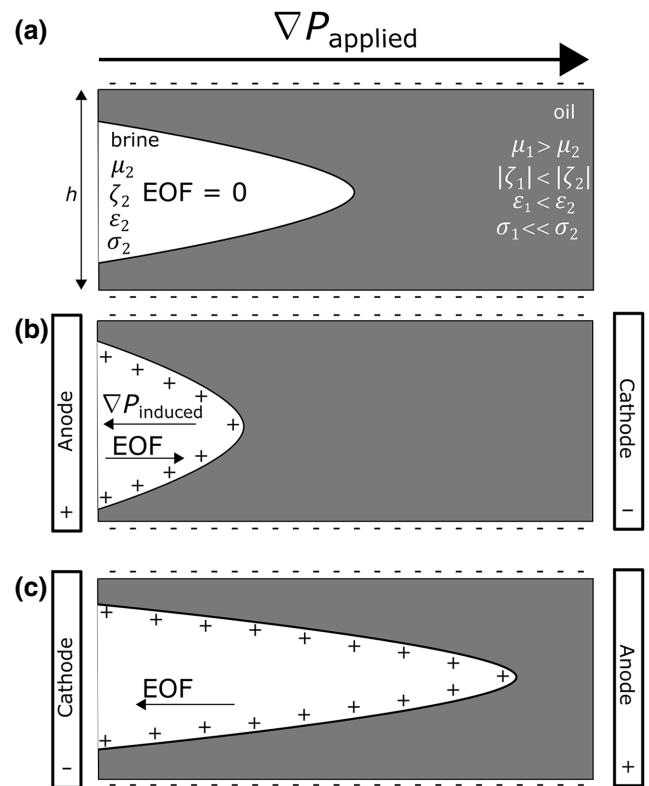


FIG. 4. Schematic representation of the electrokinetic effects at play, side view. In all cases the applied pressure gradient is from inlet to outlet as indicated. (a) Base-case situation without an electric field applied, in which a parabolic flow of the low viscosity brine develops into the high viscosity oil. (b) Under the application of a positive electric field, EOF in the direction of the pressure-driven flow develops in the brine and encounters a “dead-end pore” in the oil phase inducing a pressure gradient countering the externally applied pressure, stabilizing the displacement. (c) A negative electric field induces EOF towards the inlet, increasing instabilities within the system.

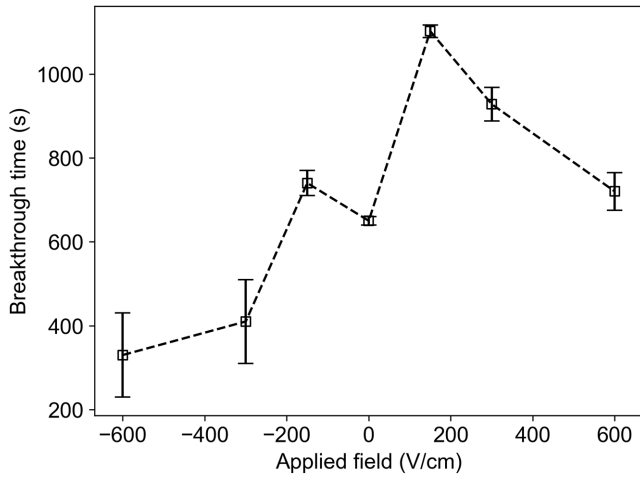


FIG. 5. Breakthrough time (seconds) for different electric field configurations. Error bars indicate the standard deviation over three experiments, lines are to guide the eye.

equal to h . There is no EDL present in the oil (gray) phase, while upon entering an EDL arises within the brine phase. Under purely pressure-driven flow [Fig. 4(a)], the displacement is inherently unstable because of the unfavorable viscosity ratio between the fluids. When a positive electric field is applied [Fig. 4(b)], EOF in the brine phase is towards the oil phase, and this EOF induces a pressure gradient in the brine as it encounters the oil. This pressure gradient then results in a reduced effective flow of the brine and reduces the viscous fingering. For the electric field in the negative direction [Fig. 4(c)], the EOF is induced towards the inlet, effectively further thickening the defending fluid and thus increasing the overall instabilities in the system since the viscosity ratio becomes even more unfavorable. This thickening of the resident fluid affects the overall pressure gradient within the system, such that the invading fluid now has an increased mobility compared to the case of a purely pressure driven flow. Due to this increased invading fluid mobility, the effective interfacial tension is also reduced.

Breakthrough times for the different electric field values are shown in Fig. 5, where we observe shorter breakthrough time for the negative electric field values compared to the positive values. The breakthrough time is defined as the time it takes for the brine to reach the outlet of the cell. Typically, a smaller breakthrough time indicates a more destabilized flow. These results are consistent with the patterns shown in Figs. 3(a)–3(g), where we observe that for an electric field of -600 V/cm for instance, the brine reaches the outlet region faster than other negative electric field values even at the same time considered.

A. Stability indices

To further scrutinize the effect of the electric field on the development of VF, the images are analyzed and three

stability indices are evaluated at breakthrough time for their respective experiments. The stability indices, which are computed using our PYTHON code, are (1) fractal dimension, (2) swept area (%), and (3) the interfacial length (pixels). The fractal dimension is a numerical value that is used to characterize fractals such as those formed in viscous fingering. Because these fractals can either grow or shrink, the fractal dimension provides a way to study the morphology and pattern of fingers [52,53]. A high fractal dimension indicates a more stable displacement [20,54–56]. The swept area is the percentage of the cell that contains the displacing fluid. In this case, a higher percentage of the swept area typically indicates a more stable displacement. Finally, the interfacial length is defined as the length of the interface between the displaced and displacing fluid, where a higher interfacial length normally indicates a highly ramified interfacial pattern and hence, a more unstable displacement [57–59]. For details on the calculations of these stability indices, see Appendix A.

The fractal dimension for the different electric fields applied is shown in Fig. 6, where it can be observed that applying a positive electric field has significantly increased the fractal dimension, indicating a more stable displacement. On the other hand, applying a negative electric field decreases the fractal dimension, which indicates an increased interfacial instability, as observed from the images in Fig. 3 as well. There are no clear trends to be observed with changing the field strengths, indicating that all positive field strengths improve the stability while all negative field strengths increase VF, but that the magnitude of the field strength has limited impact on the control of VF. This further indicates that even if the field strength is below the theoretical critical field strength, there can be significant alterations on the stability of the displacement.

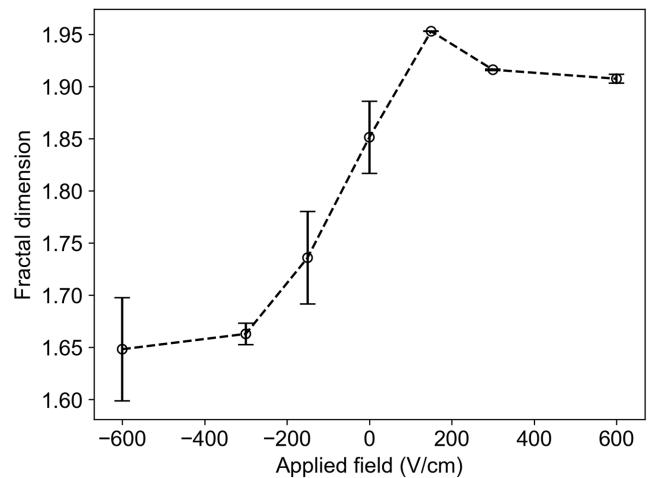


FIG. 6. Average fractal dimension at breakthrough as a function of the applied electric field. Error bars represent standard deviation over three experiments, lines are to guide the eye.

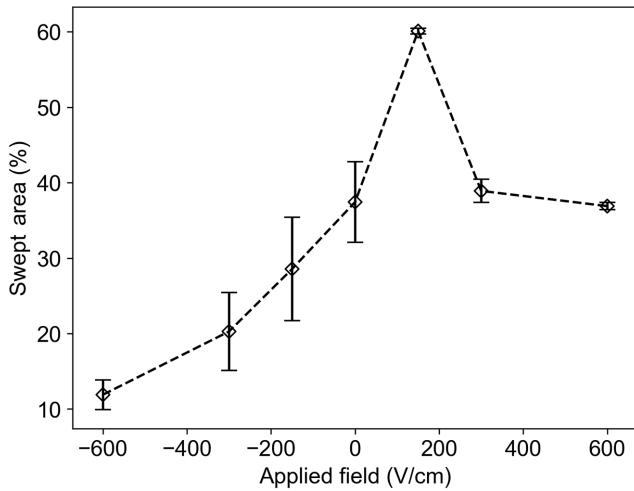


FIG. 7. Percentage of area of the cell swept by the invading brine fluid as a function of the applied electric field. Error bars represent standard deviation over three experiments, lines are to guide the eye.

The second stability index we evaluate is the percentage of the cell that is swept by the invading brine at the time of breakthrough (Fig. 7). From this figure, we can see that applying a positive field increased (+150 V/cm), or remained the same overall swept area when compared to purely pressure-driven flow (300 and 600 V/cm). On the other hand, applying a negative electric field has a significantly negative impact on the area swept at breakthrough time. In this case, the lowest value is observed at the most negative electric field strength (-600 V/cm), indicating that at this field strength the overall instability is increased most and the displacement is least effective. For large positive fields, (+300 V/cm and +600 V/cm) the swept area is not significantly changed from the purely driven flow, which is attributed to the relatively limited development of instabilities in the cell at purely pressure-driven flow because of the size limitations of our cell.

When looking at the interfacial length between the resident and invading fluid (Fig. 8) a clear echo from the other instability indices can be observed. In the case of a negative electric field, the interfacial length is significantly increased, indicating a more unstable displacement. In addition to the magnitude being increased, the error in the interfacial length is also increased significantly, indicating a larger difference between different runs as a result of the overall increased instability. On the other hand, for all positive electric field strengths a clear reduction of both the interfacial length and the errors in the interfacial length can be observed. This is further indication that the positive electric field is able to reduce the interfacial instabilities in the case of a nonconducting oil being displaced by a highly conducting brine of lower viscosity.

All these quantitative stability indices are consistent with the qualitative observations from Fig. 3, and further

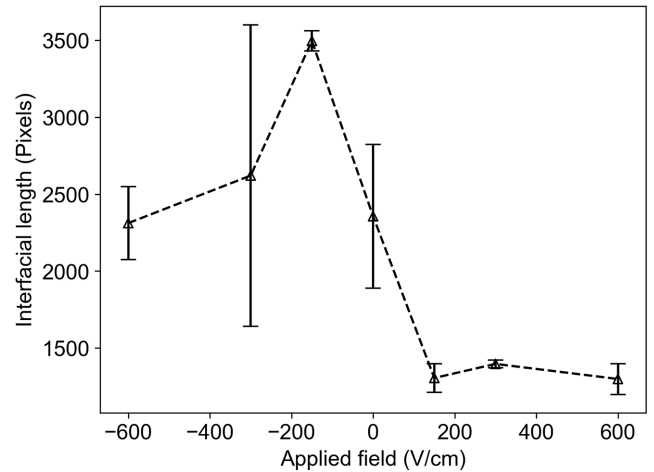


FIG. 8. Average interfacial length between the invading and defending fluid at breakthrough as a function of the applied electric field. Error bars represent standard deviation over three experiments, lines are to guide the eye.

underline that an electric field has a significant influence on the development of interfacial instabilities, even in the case of a nonconducting resident fluid. The direction of the applied electric field is highly relevant, while the magnitude of the electric field has limited influence on the stability indices. In a system in which the wall charge is negative, indicating a positive EDL, and the defending fluid is a more viscous nonconducting oil, a positive electric field (meaning an anode at the fluid inlet and a cathode at the fluid outlet) has a stabilizing effect on the instabilities, while a negative electric field destabilizes the flow significantly.

IV. CONCLUSIONS

In this experimental study, we show that electrokinetic control of viscous fingering is feasible for systems where the highly viscous defending fluid is electrically nonconducting and the invading fluid is an electrolyte. Our results clearly show an increasing interface stability when an electric field is applied in the direction of the pressure-driven flow, and EOF is induced into the same direction. Effectively, this results in a pressure buildup at the oil-water interface and an effective increase in interfacial tension as a result of the jump in conductivity across this boundary and the limited electro-osmotic mobility of the oil phase. The EOF induced in the brine layer and the zero EOF in the oil phase then builds up a pressure at the interface, effectively reducing the overall invading flow of the brine into the system. This results in the stabilization of the interface and suppression of viscous fingering. These findings are in clear contradiction with the predictions for systems containing two electrolytes of the same conductivity, but are of relevance for many applications such as the recovery of

hydrocarbons from porous reservoirs. In systems such as ours where a polar conducting fluid displaces a nonpolar resident fluid of higher viscosity, a back pressure induced by the resident oil, which acts as a “wall” in the case of positive electric fields, results in a smoother interfacial pattern, while a more irregular pattern caused by a negative EOF further destabilizes the flow.

Different stability indices are used to quantify the effectiveness of using an electric field to suppress instabilities, showing that the direction of the applied electric field is of significant influence on the stabilization and destabilization, while the magnitude of the electric field is of less relevance. In none of our experiments did we observe a fully stabilized and pistonlike displacement, indicating that even though we are increasing the stability of the interface, the interfacial phenomena leading to VF are not fully suppressed at the field strengths we investigate.

In conclusion, active control of VF through the application of an electric field is feasible in systems containing two fluids of significant different polarity. The required direction of the electric field to control the instability is dependent on the nature of the fluids and surface charge of the porous medium while the magnitude of the electric field is of limited influence on the stability of displacement. Our results are of relevance for a wide range of applications in which the polarity of resident fluids is not tunable and where the resident fluid is nonconducting.

ACKNOWLEDGMENTS

The authors of this work thank Canada First Research Excellence Fund (CFREF) for providing the funding for this research. We also wish to express our profound gratitude to Dr. Jingyi Wang and Imad Assaf, PEng (Southern Alberta Institute of Technology) for their useful advice in designing the setup used for the experiments.

APPENDIX A: METHODOLOGY FOR THE DETERMINATION OF INTERFACIAL STABILITY

Figure 9 shows the flow chart that is used in the PYTHON code for the stability indices’ determination. These stability indices are the Fractal dimension, percentage swept area, nondimensional interfacial velocity, and finally, the interfacial length. For the fractal dimension, the PYTHON

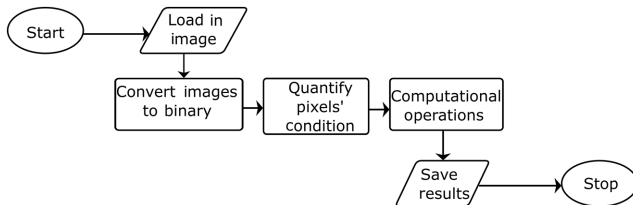


FIG. 9. General methodology of PYTHON code for image processing.

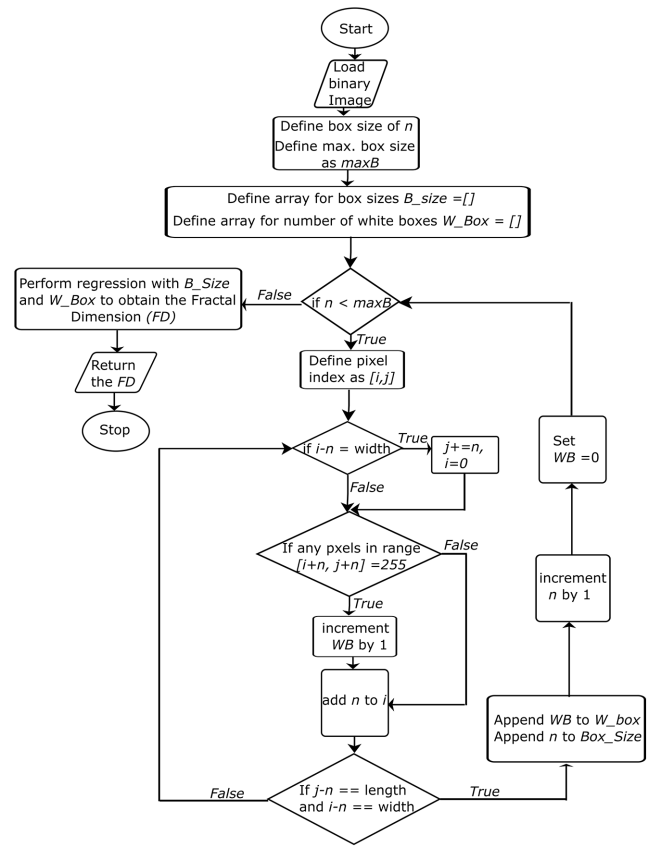


FIG. 10. Flow chart for computational determination of the box dimension.

code stores the number of boxes that has white pixels as discrete box sizes in two arrays (Fig. 10). The fractal dimension is then estimated by examining a grid of different box sizes, which consists of $S \times S$ pixel dimensions and then identifying the amount of boxes (N) that contain the viscous fingering pattern. The equation used for this calculation is shown in Eq. (A1). The percentage swept area is calculated by dividing the white pixels, which represents the invading fluid, by the total pixels as shown in

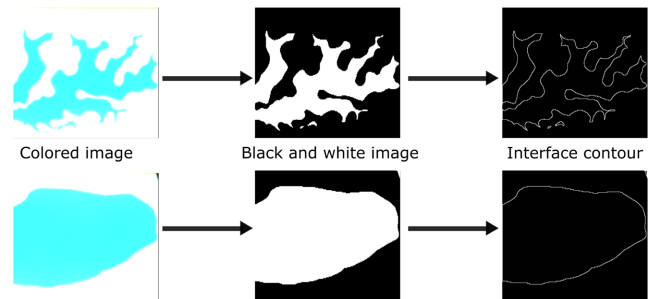


FIG. 11. Displacement pattern of -150 V/cm (top image) and $+150$ V/cm (bottom image).

Eq. (A2). The interfacial length is calculated by first creating a contour image of the mineral–oil–water interfaces. To determine the validity of a pixel located at the interface, the interface is examined by quantifying the condition of the neighboring pixels. If the surrounding pixels met a set of conditions then the pixel is considered to be an interfacial pixel and would be white in the contour image. Likewise if a pixel did not meet the interface condition it would be black in the final contour image. After the contour image is obtained the white pixels, or the interface pixels are summed. An example of the resulting contour of the image from this process is shown in Fig. 11. To calculate the nondimensional interfacial velocity (U_{ind}), the interfacial length is divided by the time stamp, and then divided by the injection velocity as shown in Eq. (A3).

$$D = -\frac{\log(N)}{\log(S)}, \tag{A1}$$

$$A = \frac{\text{Pixels}_{\text{invading fluid}}}{\text{Pixels}_{\text{total}}} \times 100\%, \tag{A2}$$

$$U_{ind} = \frac{\text{Interfacial length}}{\text{Time}} \times \frac{\text{Cross-section area}}{\text{Flow rate}} \times \text{Metric pixel conversion.} \tag{A3}$$

APPENDIX B: REQUIRED THEORETICAL FIELD STRENGTH

The table referred to in Sec. II of the main text are presented here in Table I.

TABLE I. Sensitivity analysis at different ζ -potential values for the critical electric field values required for the stabilization or destabilization of the interface based on Gao *et al.* [35].

Ca	ζ potential (mV)	E_{crit} (V/cm)
1.13×10^{-4}	-5	-1.48×10^4
1.13×10^{-4}	-70	-7.38×10^3

[1] P. G. Saffman and G. I. Taylor, The penetration of a fluid into a porous medium or Hele-Shaw cell containing a more viscous liquid, *Proc. R. Soc. Lond. A. Math. Phys. Sci.* **245**, 312 (1958).
 [2] V. Joekar-Niasar and S. Hassanizadeh, Analysis of fundamentals of two-phase flow in porous media using dynamic pore-network models: A review, *Crit. Rev. Environ. Sci. Technol.* **42**, 1895 (2012).
 [3] M. Sahimi, *Flow and Transport in Porous Media and Fractured Rock: From Classical Methods to Modern Approaches* (John Wiley & Sons, Weinheim, Germany, 2011).

[4] S. E. Buckley and M. Leverett, Mechanism of fluid displacement in sands, *Trans. AIME* **146**, 107 (1942).
 [5] M. Blunt, F. J. Fayers, and F. M. Orr Jr, Carbon dioxide in enhanced oil recovery, *Energy Convers. Manage.* **34**, 1197 (1993).
 [6] H. Ott and S. Berg, Stability analysis of CO₂-brine immiscible displacement, EGUGA, 12013 (2012).
 [7] H. E. Huppert and J. A. Neufeld, The fluid mechanics of carbon dioxide sequestration, *Annu. Rev. Fluid Mech.* **46**, 255 (2014).
 [8] Y. Cinar, A. Riaz, and H. A. Tchelepi, Experimental study of CO₂ injection into saline formations, *Soc. Pet. Eng. J.* **14**, 588 (2009).
 [9] S. Berg and H. Ott, Stability of CO₂-brine immiscible displacement, *Int. J. Greenhouse Gas Control* **11**, 188 (2012).
 [10] M. Hekmatzadeh, M. Dadvar, and M. Sahimi, Pore-network simulation of unstable miscible displacements in porous media, *Transp. Porous Media* **113**, 511 (2016).
 [11] V. Kretz, P. Berest, J. Hulin, and D. Salin, An experimental study of the effects of density and viscosity contrasts on macrodispersion in porous media, *Water Resour. Res.* **39**, 1032 (2003).
 [12] M. Wood, C. T. Simmons, and J. Hutson, A breakthrough curve analysis of unstable density-driven flow and transport in homogeneous porous media, *Water Resour. Res.* **40**, 1 (2004).
 [13] K. J. Mayfield, R. A. Shalliker, H. J. Catchpoole, A. P. Sweeney, V. Wong, and G. Guiochon, Viscous fingering induced flow instability in multidimensional liquid chromatography, *J. Chromatogr. A* **1080**, 124 (2005).
 [14] C. B. Castells and R. C. Castells, Peak distortion in reversed-phase liquid chromatography as a consequence of viscosity differences between sample solvent and mobile phase, *J. Chromatogr. A* **805**, 55 (1998).
 [15] G. Rousseaux, A. De Wit, and M. Martin, Viscous fingering in packed chromatographic columns: Linear stability analysis, *J. Chromatogr. A* **1149**, 254 (2007).
 [16] D. Pihler-Puzović, P. Illien, M. Heil, and A. Juel, Suppression of Complex Fingerlike Patterns at the Interface Between Air and a Viscous Fluid by Elastic Membranes, *Phys. Rev. Lett.* **108**, 074502 (2012).
 [17] T. T. Al-Housseiny, I. C. Christov, and H. A. Stone, Two-Phase Fluid Displacement and Interfacial Instabilities Under Elastic Membranes, *Phys. Rev. Lett.* **111**, 034502 (2013).
 [18] D. Pihler-Puzovic, R. Périllat, M. Russell, A. Juel, and M. Heil, Modelling the suppression of viscous fingering in elastic-walled Hele-Shaw cells, *J. Fluid Mech.* **731**, 162 (2013).
 [19] B. Zhao, C. W. MacMinn, and R. Juanes, Wettability control on multiphase flow in patterned microfluidics, *Proc. Natl. Acad. Sci.* **113**, 10251 (2016).
 [20] R. Holtzman and E. Segre, Wettability Stabilizes Fluid Invasion into Porous Media via Nonlocal, Cooperative Pore Filling, *Phys. Rev. Lett.* **115**, 164501 (2015).
 [21] M. Trojer, M. L. Szulcowski, and R. Juanes, Stabilizing Fluid-Fluid Displacements in Porous Media Through Wettability Alteration, *Phys. Rev. Appl.* **3**, 054008 (2015).
 [22] R. Hu, J. Wan, Z. Yang, Y.-F. Chen, and T. Tokunaga, Wettability and flow rate impacts on immiscible displacement: A theoretical model, *Geophys. Res. Lett.* **45**, 3077 (2018).

- [23] B. Xu, Y. Yortsos, and D. Salin, Invasion percolation with viscous forces, *Phys. Rev. E* **57**, 739 (1998).
- [24] H. S. Rabbani, D. Or, Y. Liu, C.-Y. Lai, N. B. Lu, S. S. Datta, H. A. Stone, and N. Shokri, Suppressing viscous fingering in structured porous media, *Proc. Natl. Acad. Sci.* **115**, 4833 (2018).
- [25] D. Bratsun and R. Siraev, in *Actuators MDPI*, 2019, Vol. 9, p. 2.
- [26] H. Zhao, J. Casademunt, C. Yeung, and J. Maher, Perturbing Hele-Shaw flow with a small gap gradient, *Phys. Rev. A* **45**, 2455 (1992).
- [27] T. Maxworthy, Experimental study of interface instability in a Hele-Shaw cell, *Phys. Rev. A* **39**, 5863 (1989).
- [28] T. T. Al-Housseiny, P. A. Tsai, and H. A. Stone, Control of interfacial instabilities using flow geometry, *NatPh* **8**, 747 (2012).
- [29] T. T. Al-Housseiny and H. A. Stone, Controlling viscous fingering in tapered Hele-Shaw cells, *Phys. Fluids* **25**, 092102 (2013).
- [30] E. Dias and J. Miranda, Taper-induced control of viscous fingering in variable-gap Hele-Shaw flows., *Phys. Rev. E* **87**, 053015 (2013).
- [31] S. Mei, J. L. Bryan, and A. Kantzas, in *SPE Heavy Oil Conference Canada* (Society of Petroleum Engineers, Calgary, Alberta, Canada, 2012).
- [32] E. Brener, D. Kessler, H. Levine, and W.-J. Rappe, Selection of the viscous finger in the 90 geometry, *EPL (Europhysics Letters)* **13**, 161 (1990).
- [33] S. Li, J. S. Lowengrub, J. Fontana, and P. Palffy-Muhoray, Control of Viscous Fingering Patterns in a Radial Hele-Shaw Cell, *Phys. Rev. Lett.* **102**, 174501 (2009).
- [34] C.-Y. Chen, C.-W. Huang, L.-C. Wang, and J. A. Miranda, Controlling radial fingering patterns in miscible confined flows, *Phys. Rev. E* **82**, 056308 (2010).
- [35] T. Gao, M. Mirzadeh, P. Bai, K. M. Conforti, and M. Z. Bazant, Active control of viscous fingering using electric fields, *Nat. Commun.* **10**, 1 (2019).
- [36] M. Mirzadeh and M. Z. Bazant, Electrokinetic Control of Viscous Fingering, *Phys. Rev. Lett.* **119**, 174501 (2017).
- [37] B. Ray, P. Reddy, D. Bandyopadhyay, S. W. Joo, A. Sharma, S. Qian, and G. Biswas, Instabilities in free-surface electroosmotic flows, *Theor. Comput. Fluid Dyn.* **26**, 311 (2012).
- [38] S. K. Kalpathy, Electrocapillary effect in liquid films with an electrically charged interface, *Mater. Today: Proc.* **44**, 3006 (2021).
- [39] D. Bensimon, Stability of viscous fingering, *Phys. Rev. A* **33**, 1302 (1986).
- [40] M. Jung, M. Brinkmann, R. Seemann, T. Hiller, M. S. de La Lama, and S. Herminghaus, Wettability controls slow immiscible displacement through local interfacial instabilities, *Phys. Rev. Fluids* **1**, 074202 (2016).
- [41] S. K. Kalpathy, Interplay of substrate wettability and surfactant distributions in controlling interfacial instability, *Eur. J. Mechanics-B/Fluids* **78**, 203 (2019).
- [42] J. Stokes, D. Weitz, J. P. Gollub, A. Dougherty, M. Robbins, P. Chaikin, and H. Lindsay, Interfacial Stability of Immiscible Displacement in a Porous Medium, *Phys. Rev. Lett.* **57**, 1718 (1986).
- [43] C. Odier, B. Levaché, E. Santanach-Carreras, and D. Bartolo, Forced Imbibition in Porous Media: A Fourfold Scenario, *Phys. Rev. Lett.* **119**, 208005 (2017).
- [44] F. Paratore, E. Boyko, G. V. Kaigala, and M. Bercovici, Electroosmotic Flow Dipole: Experimental Observation and Flow Field Patterning, *Phys. Rev. Lett.* **122**, 224502 (2019).
- [45] C. Yang and D. Yan, in *Encyclopedia of Microfluidics and Nanofluidics*, edited by D. Li (Springer US, Boston, MA, 2008), p. 266.
- [46] M. Mirzadeh, T. Zhou, M. A. Amooie, D. Fraggadakis, T. R. Ferguson, and M. Z. Bazant, Vortices of electro-osmotic flow in heterogeneous porous media, *Phys. Rev. Fluids* **5**, 103701 (2020).
- [47] H. Mahani, A. L. Keya, S. Berg, W.-B. Bartels, R. Nasralla, and W. R. Rossen, Insights into the mechanism of wettability alteration by low-salinity flooding (LSF) in carbonates, *Energy Fuels* **29**, 1352 (2015).
- [48] H. Falahati, L. Wong, L. Davarpanah, A. Garg, P. Schmitz, and D. P. Barz, The zeta potential of PMMA in contact with electrolytes of various conditions: Theoretical and experimental investigation, *Electrophoresis* **35**, 870 (2014).
- [49] S. L. Walker, S. Bhattacharjee, E. M. Hoek, and M. Elimielech, A novel asymmetric clamping cell for measuring streaming potential of flat surfaces, *Langmuir* **18**, 2193 (2002).
- [50] M. Khademi, W. Wang, W. Reitingner, and D. P. Barz, Zeta potential of poly (methyl methacrylate)(PMMA) in contact with aqueous electrolyte-surfactant solutions, *Langmuir* **33**, 10473 (2017).
- [51] K. Fa, V. K. Paruchuri, S. C. Brown, B. M. Moudgil, and J. D. Miller, The significance of electrokinetic characterization for interpreting interfacial phenomena at planar, macroscopic interfaces, *Phys. Chem. Chem. Phys.* **7**, 678 (2005).
- [52] M.-N. Pons, E. Weisser, H. Vivier, and D. Boger, Characterization of viscous fingering in a radial Hele-Shaw cell by image analysis, *Exp. Fluids* **26**, 153 (1999).
- [53] M. E. Thrasher, Ph.D. thesis, 2007.
- [54] J.-h. Zhang and Z.-h. Liu, Study of the relationship between fractal dimension and viscosity ratio for viscous fingering with a modified DLA model, *J. Pet. Sci. Eng.* **21**, 123 (1998).
- [55] P. King, The fractal nature of viscous fingering in porous media, *J. Phys. A: Math. Gen.* **20**, L529 (1987).
- [56] B. K. Primkulov, A. A. Pahlavan, X. Fu, B. Zhao, C. W. MacMinn, and R. Juanes, Signatures of fluid-fluid displacement in porous media: Wettability, patterns and pressures, *J. Fluid Mech.* **875**, R4 (2019).
- [57] L. Xia, Morphology of flow patterns generated by viscous fingering from miscible fluids, arXiv preprint arXiv:1809.09460 (2018).
- [58] C.-Y. Chen and E. Meiburg, Miscible porous media displacements in the quarter five-spot configuration. Part 1. The homogeneous case, *J. Fluid Mech.* **371**, 233 (1998).
- [59] M. Mishra, M. Martin, and A. De Wit, Differences in miscible viscous fingering of finite width slices with positive or negative log-mobility ratio, *Phys. Rev. E* **78**, 066306 (2008).